University Library

MINERVA ACCESS

A gateway to Melbourne's research publications

Minerva Access is the Institutional Repository of The University of Melbourne

Author/s:
Li, Q;Miramini, S;Smith, DW;Gardiner, BS;Zhang, L

Title:
Osteochondral junction leakage and cartilage joint lubrication

Date:
2023-03-01

Citation:
Li, Q., Miramini, S., Smith, D. W., Gardiner, B. S. & Zhang, L. (2023). Osteochondral junction leakage and cartilage joint lubrication. Computer Methods and Programs in Biomedicine, 230, https://doi.org/10.1016/j.cmpb.2023.107353.

Persistent Link:
https://hdl.handle.net/11343/332464

License:
CC BY

Revised Manuscript clean version (Without Track changes) Click here to view linked References

Title: Osteochondral junction leakage and cartilage joint lubrication

Authors: Qin Li[1], Saeed Miramini[1], David W. Smith[2], Bruce S. Gardiner[3], Lihai Zhang[1,*]

[1] Department of Infrastructure Engineering, The University of Melbourne, VIC, 3010, Australia

[2] School of Physics, Mathematics and Computing, The University of Western Australia, WA, 6009, Australia

[3] Centre for Molecular Medicine and Innovative Therapeutics, Murdoch University, WA, 6150, Australia

* Corresponding author (Email: lihzhang@unimelb.edu.au)

Highlights:

- Effect of osteochondral junction leakage on cartilage tissue lubrication

Abstract

Background and Objectives: Previous studies have shown that there is potentially interstitial fluid exchange between cartilage tissue and the subarticular spongiosa region in the case of injury or disease (*e.g.,* osteoarthritis and osteoporosis). Interstitial flow is also required for cartilage lubrication under joint load. A key question then is how cartilage lubrication is modified by increased interstitial fluid leakage across the osteochondral junction. Thus, the purpose of this study is to develop a numerical model to investigate changes in cartilage lubrication with changes in osteochondral junction leakage.

Methods: The multi-phase coupled model includes domains corresponding to the contact gap, cartilage tissue and subchondral bone plate region (ScBP). Each of these domains are treated as poroelastic systems, with their coupling implemented through mass and pressure continuity. The effects of osteochondral junction leakage on lubrication were investigated with a parametric study on the relative permeability between the ScBP and cartilage tissue.

Results: Significant effects of ScBP permeability were predicted, especially during the early stage of the junction leakage development (early stage of the disease). There is a significant reduction in mixed-mode lubrication duration under the effect of increased junction leakage (the cartilage tissue mixed-mode lubrication duration is about 33% decrease for a relative permeability ratio of 0.1 between ScBP and cartilage tissue, and about 52% decrease under the osteoarthritis condition). In addition, the time for cartilage to reach steady-state consolidation is significantly reduced when ScBP permeability increases (the consolidation time reduces from roughly 2 hours to 1.2 hours when the relative permeability ratio increases from 0.001 to 0.1, and it reduces to 0.8 hours for an advanced osteoarthritis condition). It is predicted that the initial friction coefficient could increase by over 60% when the ScBP permeability is consistent with an advanced osteoarthritis (OA) condition.

Conclusion: Increased osteochondral junction leakage induced by joint injury and disease could result in increased cartilage surface wear rates due to more rapid interstitial fluid depressurization within articular cartilage.

Keywords: Cartilage; subchondral bone plate region; osteochondral junction leakage; coefficient of friction; mixed-mode lubrication duration; permeability

1 Introduction

Friction force is defined as the resistance to the relative motion between two opposing surfaces. It can be the dry friction between solid components or the fluid friction caused by shear of viscous fluids, while in the case of saturated porous solids there is some combination of the two (*i.e.,* known as 'mixed mode'). In the context of articular cartilage, mixed mode lubrication usually occurs in the synovial joints between opposing cartilage surfaces [1, 2].

Articular cartilage [2], within the knee synovial joint, is a thin biological soft tissue covering the end of the tibia and femur bone where it exhibits the extraordinary characteristic of a bearing material with an ultra-low initial friction coefficient of 0.001. This outstanding lubrication outperforms the most slippery materials in the world, such as boron-aluminum-magnesium (0.02 of the friction coefficient [3]) and Teflon (0.05 of the friction coefficient [4]). The cartilage lubrication mechanisms have been studied extensively over the past decades and many theories have been proposed [5, 6]. These theories include fluid-film lubrication [7], mixed-mode lubrication [1, 8], boundary lubrication [9], biphasic lubrication [10] and weeping lubrication [11, 12] amongst others [5].

Synovial joints experience an ultralow friction coefficient at the early stage of mixed mode lubrication regime due to the pressurized interstitial fluid in the cartilage tissue; this mechanism is referred to as hydrodynamic lubrication. Under loading, the fluid exudes from the cartilage tissue resulting in load sharing between solid and fluid phases. This addition of solid-solid contact, or asperity contacts, leads to both hydrodynamic and boundary lubrication, and is known as mixed mode lubrication [2]. The mixed-mode lubrication duration in this paper is defined as the time between the initial contact of the cartilage surface asperities and 99% depletion of the gap fluid (*i.e.,* when the gap fluid pressure due to joint loading approaches to zero) [1].

Cartilage tissue normally has extremely low fluid permeability. However, the subchondral bone plate region (ScBP), which is defined as the subchondral cortical bone plate, in the canalicular region immediately beneath the cement line, including the calcified cartilage layer in this study, has a (microscale) permeability that is significantly smaller than articular cartilage under normal conditions. The calcified cartilage is the deep zone cartilage tissue that has a solid fraction comprising calcium crystals and collagen fibrils. The calcium crystals are essentially watertight, and the collagen fibrils have low permeability, and together they help

to create an impermeable or near-impermeable osteochondral boundary. This subchondral bone plate region (ScBP) is generally believed to be impermeable [13-16] for normal and healthy joints. Even though this concept has been challenged recently [17, 18], some studies still show that the impermeable or near-impermeable assumption is a good approximation for healthy young adult joints in the numerical modelling [19-23].

The studies from Martin-badosa et.al. [19] and Schneider et.al. [20, 21] suggests that the vascular porosity in femur cortical bones is found to be in the range of ~1 – 5 %, but this vascular porosity value includes the Haversian and Volkmann cannels. However the subchondral bone plate region that is immediately beneath the cement line has canalicular porosity only, so the porosity value should be around the lower end of this range in normal adult subchondral bone (i.e. in the region of less than 1% to 2%). Similarly from Pouran's measurements [22], the porosity in human chondral bone plate can be as low as 4% in elderly people (aged between 67 to 85), this value considers the possible aging effect on the bone density and the pores space arising from new Haversian and Volkmann cannals, which obviously results in a porosity higher than that of the canalicular systems alone (the region that is immediately beneath the cement line).

Malandrino et. al. [23] proposed an empirical relationship between porosity and permeability. If we assume a porosity of 1% (in young and healthy adult's joint) for the subchondral bone plate region (excluding the Haversian and Volkmann cannels region), we can estimate ScBP permeability being about $3.3 \times 10^{-19}\ m^4/Ns$ according to their empirical relationship [23], this is about 3 to 4 orders of magnitude smaller than cartilage tissue's permeability. This theoretical calculation is also consistent with Gailani et al's experimental results [24] (which suggests a even lower permeability, around $10^{-20}\ m^4/Ns$). In addition theoretical calculation confirm these low permeability estimates. Given the thickness of the subchondral bone with canalicular porosity only immediately beneath the subchondral cement line and its exceptionally low permeability, as well as the thickness of the calcified cartilage layer with a reduced permeability, it is then reasonable to assume the impermeable or near-impermeable condition for osteochondral junction region for normal adult joints.

However, the impermeable (or nearly impermeable) assumption is unlikely to be accurate for older people, particularly those with osteoarthritic joints. As shown in Hwang's experiment [25], in the osteochondral junction of patients with the average age of 70 years old requiring

arthroplasty due to OA, the permeability in the subchondral bone plate region (cortical bone plate plus CCZ) is at least 350 – 600 times greater than the permeability of the hyaline cartilage tissue itself [25]. Even larger increases, of several orders of magnitude has been reported for increases in vertebral end-plate permeability with age [26]. Together these findings suggest that the impermeable boundary condition at the osteochondral junction is probably inaccurate in aged and especially in joints with advanaced osteoarthrosis [17]. We therefore consider fluid leakage through the osteochondral junction as a result of aging and/or disease states, and its effect on joint lubrication.

Increased fluid leakage at the osteochondral junction may compromise cartilage lubrication at the contacting surfaces, as osteochondral leakage provides an extra drainage pathway as the articular cartilage consolidates, and also reduces the drainage path length, so again increasing the cartilage tissue drainage rate. Consequently tissue deformation and the depletion of the elevated pressurized fluid occurs more quickly when osteochondral junction leakage increases. The additional flow path will result in less fluid escaping via the contact gap, which will reduce the effect of so-named 'weeping lubrication', as proposed by McCutchen et al. [11, 12]. Reduced lubrication reduces the time that the tissue is able to sustain the physiological loading without significant cartilage surface friction, which then leaves the cartilage surface more suspectible to damage.

This paper serves as the first step toward coupling the osteochondral junction region with the cartilage tissue, and cartilage contact gap, to improve our understanding of the role subchondral bone plate permeability plays in cartilage lubrication within synovial joints. The objective of this study is to numerically investigate the effect of the permeable subchondral bone plate on cartilage lubrication behavior under osteochondral junction leakage conditions. We hypothesize that once the subchondral bone plate becomes more permeable, the lubrication capability of the cartilage tissue will deteriorate significantly. To test this hypothesis, we develop a mathematical model to simulate the lubrication and consolidation behavior of the cartilage tissue, and use the model to predict the critical parameters in cartilage lubrication including the mixed-mode lubrication duration, time-dependent peak strain, degree of consolidation, and the time-dependent friction coefficient. The friction coefficient used in this paper is the effective friction coefficient [27], which varies depending on the fluid load support. At the early stage of loading, the joint load is supported by the

pressurized fluid in the cartilage tissue resulting in minimum solid contact and very low friction; however when the pressurized fluid drains away, the solid component of the opposing cartilage tissues starts making more contacts and the effective friction coefficient then rises. In prior studies it is shown that the effective friction coefficient could reach around 0.3 at an equilibrium steady-state [27].

2 Materials and methods

2.1 Study overview and assumptions

This study presents a multi-phase coupled model of the joint under the mixed-mode lubrication regime. The model incorporates the fluid flow behavior in different regions and also the fluid interactions between these regions under physiological loading, as listed below:

- Fluid flow in the cartilage contact gap, interstitial fluid flow in the cartilage tissue, and interstitial fluid flow through the subchondral bone plate
- Fluid exchange between the contact gap and cartilage tissue, and fluid exchange between the cartilage tissue and subchondral bone plate

The contact gap model [1] considers the gap fluid flow based on gap permeability and surface asperity deformation during gap closure with fluid exchange between tissue and contact gap. The cartilage tissue model [28] considers the fluid flow based on Darcy's Law. The subchondral bone plate model considers the fluid flow based on Darcy's Law, with permeability of the subchondral cortical bone K_{ScBP} being a portion of the cartilage tissue permeability K_c.

In this study, we aim to investigate the effect of the potential for a defective osteochondral junction to influence tissue lubrication at the contacting surfaces, by increasing the relative permeability of the subchondral bone plate from a normal condition (with a near impermeable state, $K_{ScBP}/K_c = 0.001$) towards the advanced OA condition ($K_{ScBP}/K_c \rightarrow 600$) [2, 25].

An overview of this study and the methodology is presented in figure 1, the schematic diagram showing the details of the model is given in figure 2. The model is constructed under the cylinderical coordinate system. Note that the cartilage tissue, cartilage contact gap, and subchondral bone plate are all considered as biphasic porous media and coupled in the joint lubrication system model.

The main assumptions that were used in the study are summarized as follows.

- An axis-symmetrical geometry and boundary conditions is assumed. This assumption has also been adopted in previous studies [1, 29, 30].
- An axis-symmetric coordinate is adopted, meaning that the load distribution, stress-strain response, and fluid flow behaviour will be the same in all directions in this model. It is a reasonable assumption due to the shape of the meniscus [31], and the approximately axisymmetric strain contours observed by Marzo and Gurske-DePerio under a controlled experimental condition [32].
- The viscosity, density, and molecular composition of synovial fluid and cartilage interstitial fluid is assumed to be unchanged throughout the simulation.

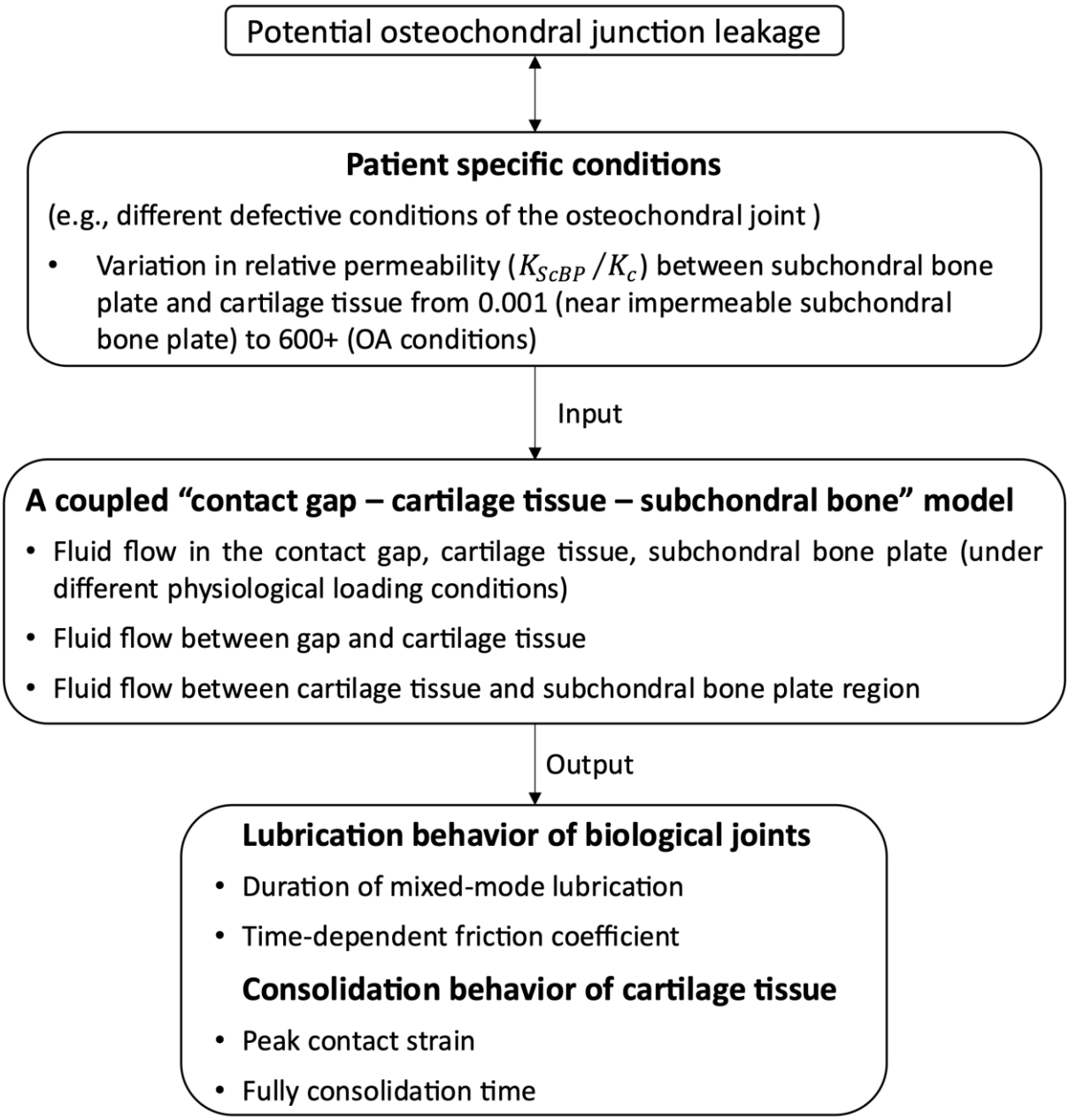


Figure 1: Schematic diagram showing the methodology used in this study

2.2 Joint multi-phase coupled model

2.2.1 Cartilage tissue poroelastic model

The authors previously published and developped the cartilage tissue model based on an upscaled porous media theorey [28-30, 33], which was validated against the *in vitro* experimental measurement [34]. The use of the porous media theory to predict cartilage

mechanical response is not a recent idea [35, 36], however its use to couple with cartilage contact gap and subchondral bone plate to form a osteochondral joint is relatively new.

Under this poroelastic theory framework, the cartilage model [28-30] encorporates the aggrecan-dependent tissue stiffness, tension-compression nonlinearity [37] and aggrecan-dependent permeability. The cartilage in the model is treated as a fully saturated porous media that has the interstitial fluid phase and solid phase (extracellular matrix) [2, 38-40].

For the force balance in the cartilage tissue model, the conservation of momentum is applied by neglecting the body and inertia forces as shown below [2, 29, 30],

$$\boldsymbol{\nabla} \cdot \boldsymbol{\sigma}_t = 0 \tag{1}$$

where $\boldsymbol{\sigma}_t$ is the total stress (cauchy stress tensors of solid and fluid) in the cartilage, given by [27, 30, 36],

$$\boldsymbol{\sigma}_t = \boldsymbol{\sigma}_{solid} + \boldsymbol{\sigma}_{fluid} = \boldsymbol{\sigma}_E^S - p_c \boldsymbol{I} \tag{2}$$

where $\boldsymbol{\sigma}_E^S$ is the incremental elastic effective stress of the deformed solid phase under loading, and p_c is the incremental intertstitial fluid pressure, and $\boldsymbol{I}$ is the identity tensor.

The solid phase constituent effective stress $\boldsymbol{\sigma}_E^S$ is given below [30],

$$\boldsymbol{\sigma}_E^S = \frac{2}{J^S} \boldsymbol{F^S} \cdot \frac{\partial U(\boldsymbol{u^S})}{\partial \boldsymbol{C^S}} \cdot \boldsymbol{F}^{ST} \tag{3}$$

where $U(\boldsymbol{u^S})$ is the stored Helmholtz energy per unit volume (i.e., strain energy density) [41], and $\boldsymbol{F^S}$ is deformation gradient, and $\boldsymbol{C^S} = \boldsymbol{F}^{ST} \times \boldsymbol{F}^S$ is right Cauchy-Green solid deformation tensor, and $J^S = \det(\boldsymbol{F}^S)$ is the volume change ratio.

The tension-compression nonlinearity of the solid matrix is considered in the model by employing the Conewise Linear Elasticity model with different tensile and compressive properties [37, 42]. The aggrecans with glycosaminoglycans of high fixed charge density induce high osmotic pressure, and hence contributing to tissue compressive stiffness under the load [27, 43]. The relationship between cartilage solid matrix compressive stiffness and aggrecan is given below based on the experimental studies [44].

$$H_A = \alpha_1 \phi_G + \alpha_2 \phi_G^2 \tag{4}$$

where H_A is the aggregate (osmotic) modulus, $\alpha_1 = 0.01\ MPa$ and $\alpha_2 = 0.075\ MPa$ are the empirical constants [44], ϕ_G is the "actual" aggrecan concentration with respect to the cartilage volume excluding the collagen volume fraction.

The "actual" aggrecan concentration ϕ_G varries with cartilage deformation and location, as given below

$$\phi_G = \frac{\phi_{G0}}{J^s - CVF} \quad \textbf{(5)}$$

where ϕ_{G0} is the depth-dependent initial "apparent" aggrecan concentration with respect to intially total cartilage volume (the values are linear interpolated between $\phi_{G0}|_{z=0} = 30\ mg/ml$ and $\phi_{G0}|_{z=5mm} = 120\ mg/ml$ [1, 45], where $z = 0$ represents the center line of cartilage surface toughness as presented in figure 2), CVF is the depth-dependent collagen volumetric fraction (45% at superficial zone, 30% at the middle zone, 25% at deep zone) [29].

The cartilage tissue compressive elastic modulus (E_c) [2] can then be calculated from the aggregate modulus as shown below

$$E_c = 3H_A(1 - 2\vartheta) \quad \textbf{(6)}$$

where ϑ is aggrecan effective poisson ratio.

The tensile stiffness of cartilage matrix (E_t) that is governed by the collagen network exhibits depth-dependent and orientation-dependent features, the values adopted in this study is summaried in below table [29, 46].

Table 1 – tensile modulus and shear modulus for cartilage [29, 46]

	Tensile modulus (Mpa)		Shear modulus (Mpa)
	Horizontal	Vertical	
Superficial zone	100	25	3
Middle zone	30	10	3
Deep zone	10	6	2

As mentioned previously, a non-linear tension-compression material model is used in the computational model to describe cartilage tissue deforamtion behaviour. Therefore, E_c describes cartilage's modulus of elasticity in compression, whereas E_t describes cartilage's modulus of elasticity in tension. Both E_c and E_t are implemented in the stiffness matrix in

the computational model, so that when a sepcific element of the tissue is under tension, E_t will be applied in the deforamtion calculation; and once when the specific element is under compression, E_c will be incorporated.

The fluid flow in the cartilage is governed continuity equation (mass conservation) and Darcy's law [47-51],

$$\boldsymbol{\nabla} \cdot (\boldsymbol{v}_d^c + \boldsymbol{v}_s) = 0 \quad \textbf{(7)}$$

$$\boldsymbol{v}_d^c = \phi_f(\boldsymbol{v}_f - \boldsymbol{v}_s) = -K_c \boldsymbol{\nabla} p_c \quad \textbf{(8)}$$

where $\boldsymbol{v}_d^c$ the fluid flux is referred to as the Darcy's velocity of the fluid within the tissue defined as the relative velocity between fluid phase $\boldsymbol{v}_f$ and solid phase $\boldsymbol{v}_s$. ϕ_f the porosity is taken as 0.8 [52]. K_c is the aggrecan dependent permeability, which takes into account of the effect of the negative charged ions on flow resistence, the empirical equation is given below based on the experimental observations [53, 54].

$$K_{\mathbf{c}} = \frac{n \cdot (\phi_G)^m}{\eta_c} \quad \textbf{(9)}$$

where n = 5.4e-22 m^2 and m = -2.37 are empirical constants. η_c is the water viscosity at 37°C (0.0007 $Pa \cdot s$).

2.2.2 The contact gap model

Authors previously developed the contact gap model and coupled it with the above cartilage tissue model, and it has been proved that this coupled model represents a more realistic joint in the mixed mode lubrication regime when the cartilage is loaded [1]. The modelling is briefly descripted below.

The model treats the contact gap as a porous medium that consists of gap fluid phase and solid phase (the interconnected pores formed by surface roughness between tibial and femur cartilage).

The fluid flow in the contact gap is governed by Darcy's law,

$$\boldsymbol{v}_d^g = -K_g \boldsymbol{\nabla} p_g \quad \textbf{(10)}$$

where $\boldsymbol{v}_d^g$ is the fluid velocity. p_g is the gap fluid pressure. K_g is the gap permeability, which is dominately determined by the gap height, surface roughness and surface aggrecan. The gap

permeability reduces as the gap is closing under the loading, and approaches to cartilage permeability when the gap is "functionally closed" (when gap height is about 1 μm) [1]. The values for gap permeability have been numerically evaluated based on the computational fluid dynamics model against the experimentally measured bovine cartilage surface roughness, the details can be found in previous studies [1, 55].

The fluid flows, fluid exchange (between contact gap and cartilage tissue) and gap deformation (surface asperity and gap size) are governed by the mass conservation,

$$\frac{\partial \varepsilon_v^g}{\partial t} + \nabla \cdot v_d^g = s \tag{11}$$

where s is the rate of change of the fluid exchange per unit volume, $\frac{\partial \varepsilon_v^g}{\partial t}$ is the rate of change of contact gap volumetric strain, the volumetric strain of the contact gap is related to the gap height h, the constitutive relationship for the gap height h and total stress $\boldsymbol{\sigma}_t$ was proposed based on experimental studies for the human cartilage [56, 57].

$$h = h_0 e^{\sigma_c/\beta} = h_0 e^{\sigma_T + p_g/\beta} \tag{12}$$

where $h_0 = 9\ \mu m$ is the undeformed gap height at the beginning of the loading, σ_c is the surface asperity contact stress, $\sigma_T = \sigma_c - p_g$ is the total applied stress which is resisted by the solid contact stress (σ_c) and fluid pressure in the gap (p_g), β is the stiffness for the cartilage surface asperity (taken as 20% of the aggregate modulus) [1, 58].

By integrating the mass conservation equation with the above equations, the governing equation at the contact gap in cylindrical coordinates can be obtained as below [1],

$$\frac{1}{\beta}\frac{dp_g}{dt} = \frac{\partial}{\partial r} K_g \frac{\partial p_g}{\partial r} + \frac{K_g}{r}\frac{\partial p_g}{\partial r} + \frac{u_{dv}^c}{h_0 e^{(\sigma_t + p_g)/\beta}} \tag{13}$$

where u_{dv}^c is the normal component of fluid velocity within the cartilage at the interface between contact gap and cartilage tissue.

2.2.3 The subchondral bone plate model

The subchondral bone plate is modelled as another layer of porous medium underneath the cartilage tissue model by considering different material properties as compared to cartilage tissue.

The continuity equation in the region is given as,

$$\boldsymbol{\nabla} \cdot (\boldsymbol{v}_{\boldsymbol{f}}^{scbp} + \boldsymbol{v}_{\boldsymbol{s}}) = 0 \quad \textbf{(14)}$$

where $\boldsymbol{v}_{\boldsymbol{f}}^{ScBP}$ is Darcy's velocity in the subchondral bone plate,

$$\boldsymbol{v}_{\boldsymbol{d}}^{ScBP} = -K_{ScBP}\boldsymbol{\nabla} p_{ScBP} \quad \textbf{(15)}$$

where K_{ScBP} is the ScBP permeability which is taken as a portion of cartilage tissue permeability in the current study, $\boldsymbol{\nabla} p_{ScBP}$ is the pressure gradient.

The momentum equation is given as

$$\boldsymbol{\nabla} \cdot \boldsymbol{\sigma}_t = 0 \quad \textbf{(16)}$$

The total stress $\boldsymbol{\sigma}_t$ is supported by both the solid and fluid component,

$$\boldsymbol{\sigma}_t = \boldsymbol{\sigma}_{solid} + \boldsymbol{\sigma}_{fluid} = \boldsymbol{\sigma}_{\boldsymbol{E}}^{ScBP} - p_{ScBP}\boldsymbol{I} \quad \textbf{(17)}$$

The constitutive relation for the solid component in the ScBP region is,

$$\boldsymbol{\sigma}_{\boldsymbol{E}}^{ScBP} = E_{ScBP} \cdot \varepsilon \quad \textbf{(18)}$$

where E_{ScBP} is the Young's modulus, $\boldsymbol{\varepsilon}$ is the vertical strain, the deformation of this region is assumed to be elastic due to the large bone stiffness and relative small physiological load as compared to the strength, 1-D deformation is considered due to the relative small ScBP thickness [17, 59, 60] as compared to its cross sectional area. In fact, as expected the deformation in the bone is very small (negligible) as per calculation, hence any changes in the bone porosity with loading can be reasonably neglected in the analysis, we note that the other uncertainties such as the ScBP bone permeability is far more important in the study.

To show how the increasing ScBP permeability affects the lubrication behavior of the whole joint system, a parametric study has been performed, varying the subchondral layer from being an near impermeable barrier ($K_{ScBP}/K_c = 0.001$) to a very permeable and porous layer with relative permeability ratio larger than 600 ($K_{ScBP}/K_c > 600$). The high permeability case representes a compomised layer, through injury or disease [2, 25]. The material properties for the subchondral bone plate model are summarized in Table 2 [22, 61, 62].

Table 2 – Material properties for the subchondral bone plate used in this study [22, 61, 62]

	The Subchondral Bone Plate
Young's modulus (Mpa)	17,000
Poisson's ratio	0.3
Density (drained) (kg/m^3)	800
Fluid compressibility (Mpa)	2,300

2.3 Modelling configurations and boundary conditions

2.3.1 Model geometry

The geometry of the model that is adopted in this study was based on MRI measurements [63]. The ScBP model is constructed below the cartilage tissue, with an assumption of the thickness being 0.4 mm, which is taken from Hwang's experimental work[25]. Note, even though ScBP thickness varies depending on the location and joint condition [64, 65], the simplification of the constant thickness is reasonable for purpose of investigating how varying permeability of the subchondral bone plate region affects the cartilage tissue.

2.3.2 Loading configuration

The conically-distributed loading is adopted based on the MRI measurements [63] and experimental deformation contours [32]. This loading approach was also used in the previous study [29]. To simulate human one-leg standing, the static compression force of 970N (by assuming 2.59 body weight for a person weighs 75kg [66]) is applied at the loading intereface for more than 3 hours to achieve equilibrium condition.

2.3.3 Contact gap permeability adjustment

As shown in figure 2, multiple fluid flow paths at the contact gap are considered due to the presence of the menisci (i.e., one flow path between contact surfaces of femur and tibia cartilages, two flow paths between of femur and meniscus and tibial surface and meniscus). To account for this, the contact gap permeability in the region where has two flow paths is assumed to be doubled as compared to the region that only has one flow path.

$$\text{Gap permeability} = \begin{cases} K_g, & 0 \le r \le l_f \text{ , meniscus free region} \\ 2K_g, & l_f \le r \le l_f + l_m, \text{meniscus covered region} \end{cases} \quad \textbf{(19)}$$

2.3.4 Boundary conditions and initial conditions

The boundary conditions for the study is summarized in figure 2 B'-B' and figure 3. The total stress $\boldsymbol{\sigma}_t$ is applied on both contact gap and cartilage tissue at the contact gap and tissue

coupling interface. The pressure continuity are also imposed at the interface (figure 2 B'-B' and figure 3).

$$p_c(r,0) = p_g(r,0) \quad \textbf{(20)}$$

The continuity of normal fluid velocity u_{dv}^c is also imposed at the interface which is already accounted for in the mass conservation equation (13) in the contact gap model.

The zero pressure (ambient fluid pressure) condition is applied at the periphery edge of the contact gap.

$$p_g(r = r_0, z = 0) = 0 \quad \textbf{(21)}$$

The free flux (ambient fluid pressure) is also applied at the periphery edge of cartilage tissue as shown in figure 3.

As for the interface betwwen cartilage tissue and subchondral bone plate model, the fluid pressure and flux continuity contition is also applied.

$$p_c(r, z = Th(r)) = p_{ScBP}(r, z = Th(r)) \quad \textbf{(22)}$$

$$u_d^c(r, z = Th(r)) = u_d^{ScBP}(r, z = Th(r)) \quad \textbf{(23)}$$

where u_d^{ScBP} is the normal velocity flux at the subchondral bone plate; $Th(r)$ is the thickness of the cartilage tissue as a function of radius, the geometry of the cartilage tissue is constructed based on the MRI image [29, 63];

The subchondral trabecular bone (spongy bone) that lies below the subchondral bone plate is highly porous bone enclosing a lot of space filled with bone marrow [67, 68]. It is assumed to be an opened space to the system due to its large void ratio [69]. Therefore, the free flux boundary condition is assigned at the bottom edge of the subchondral bone plate, once the fluid can pass the subchondral bone plate, the flow resistance will be reduced significantly. The subchondral bone plate is assumed to have 0.4 mm of thickness [70].

$$p_{scbp}(r, z = -Th(r) - 0.4) = 0 \quad \textbf{(24)}$$

The fixed constraint is imposed at the bottom edge of the subchondral bone plate model.

2.3.5 Initial conditions

The numerical modeling begins with the initial contact of the surface asperities at the contact gap (for mixed mode lubrication regime). The initial contact gap fluid pressure is assigned as the total pressure at the cartilage surface (coupling interface).

$$p_g(t=0) = p_c(t=0, z=0) = -\sigma_t; \quad h(t=0) = h_0 \tag{25}$$

2.4 Numerical model settings

The numerical simulation and finite element analysis are conducted in COMSOL Multiphysics Poroelastic Module. This multiphase coupled model is constructed as a two-dimensional axisymmetric model and meshed with 1204 triangle elements. The time-dependent solver with a general relative tolerance of 0.01 is utilized to solve the governing equations.

A few relative permeability cases ($K_{scbp}/K_{cd} =$ 0.001, 0.01, 0.02, 0.03, 0.05, 0.1, 0.15, 0.2, 0.4, 0.6, 0.8, 0.9, 1, 5, 10, 50, 350, 600, 1000) were considered in this parametric study to cover the input range.

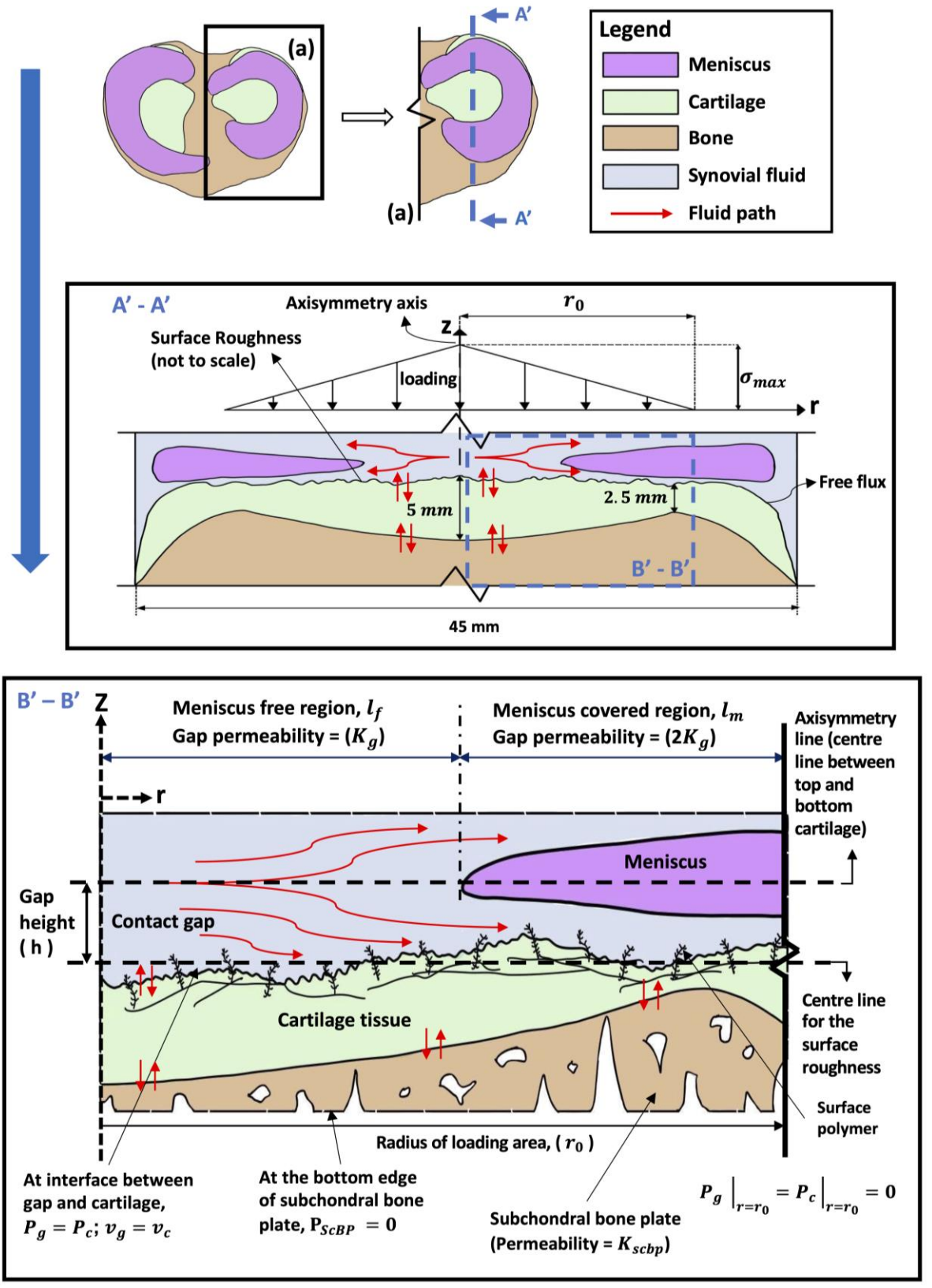


Figure 2: Schematic diagram of the current study showing the details of the fully coupled "contact gap – cartilage tissue – subchondral bone" model

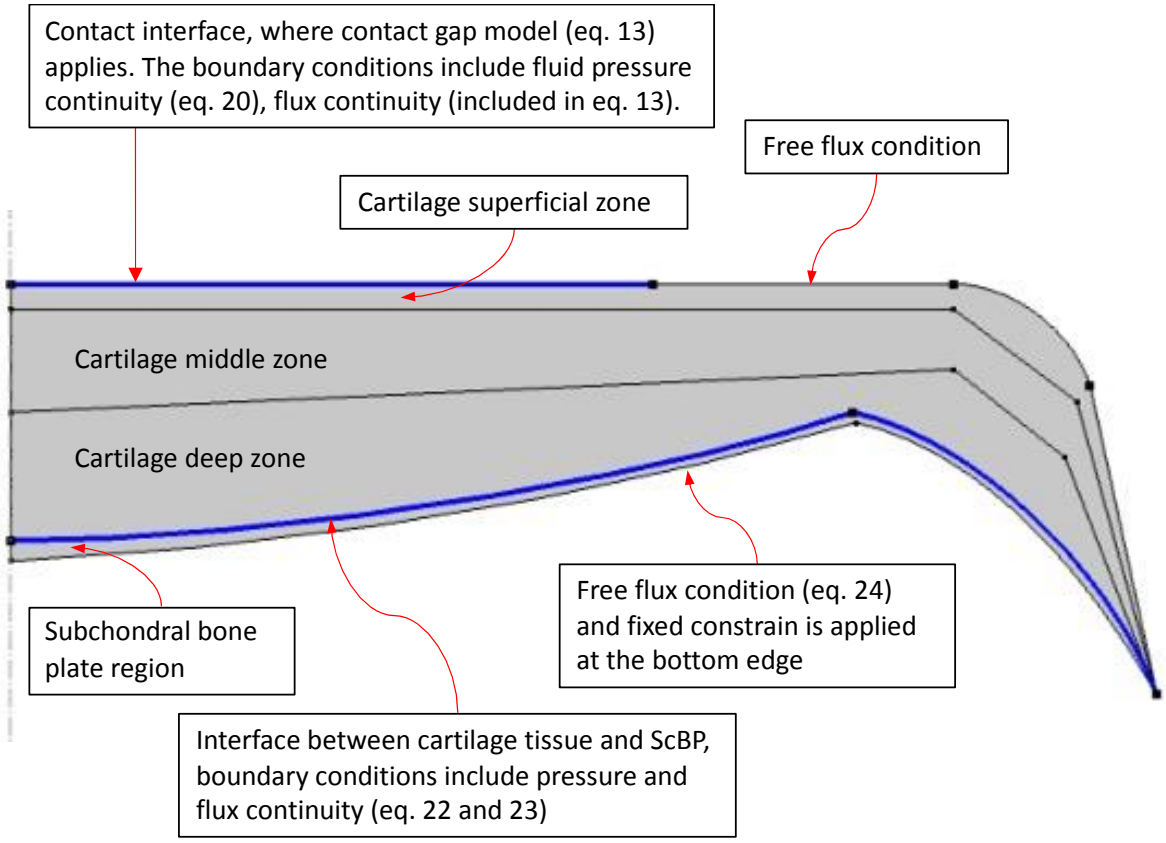


Figure 3: Boundary conditions applied on the multi-phase model

3 Results and discussion

3.1 Cartilage consolidation and deformation behaviour

Figure 4 presents how different degrees of relative permeability (K_{ScBP}/K_c) affect the cartilage tissue consolidation response. Figure 4 (a) shows the peak contact strains under different scenarios. The peak contact strain in this paper is defined as the maximum deformation of the cartilage tissue (along the axisymmetric line at the maximum stress) divided by the cartilage thickness as shown in eq. (26).

$$\varepsilon(t) = {}^{w(t)}/_{Th} \quad \textbf{(26)}$$

where $w(t)$ is time-dependent peak deformation; Th is the maximum cartilage thickness.

At the static state, the peak contact strain for all cases is approaching a constant value of around 0.28. This is consistent with the experimental measurements performed by Barker and Seedhom [34], who reported the average peak strain of 0.31 with a standard deviation

of 0.03 at the medial compartment. At times of 10s and 300s, the numerical simulation predicts the peak strain of 0.13 and 0.17 respectively, this is also close to MRI measurements [71]. The comparison between numerical modeling and experiment measurements is summarized in Table 3.

Table 3 – Comparison of peak contact strain between numerical simulation and experiment measurements.

Time (s)	Peak Contact Strain	
	Numerical modeling	Experiment measurements: mean (standard deviation)
10	0.13	0.09 (0.03) [71]
300	0.17	0.13 (0.03) [71]
Steady state	0.28	0.31 (0.03) [34]

As shown in figure 4(a), the cartilage tissue in the diseased joint (i.e. for more permeable subchondral bone plate cases) deforms much faster compared to the (normal joint) control. This is also illustrated in the consolidation curve over the time, as shown in figure 4(c), which indicates that the consolidation time reduces at the higher relative permeability cases. In other words, the cartilage system consolidates more quickly and the articular cartilage deforms at a faster rate. The degree of consolidation in this paper is defined based on the peak contact strain as shown below.

$$DoC(t) = \frac{\varepsilon(t) - \varepsilon_0}{\varepsilon_{steady\ state} - \varepsilon_0} \quad \textbf{(27)}$$

In eq. (27), $\varepsilon(t)$ is the time-dependent peak contact strain, ε_0 is the initial peak contact strain (elastic strain) and $\varepsilon_{steady\ state}$ is the strain at the steady state. Full consolidation time (i.e. steady state) is defined when 99% consolidation is reached.

It takes about 2 hours for the control case (near impermeable junction, which it is assumed to be the case for healthy young adult) to reach a fully consolidation state (99%). While the ScBP permeability increases, this steady state consolidation time reduces. For example, when the relative permeability ratio is 0.1, the full consolidation time reduces to 1.2 hours. Whereas, when the relative permeability ratio is 600, which is consistent with an OA condition, the full

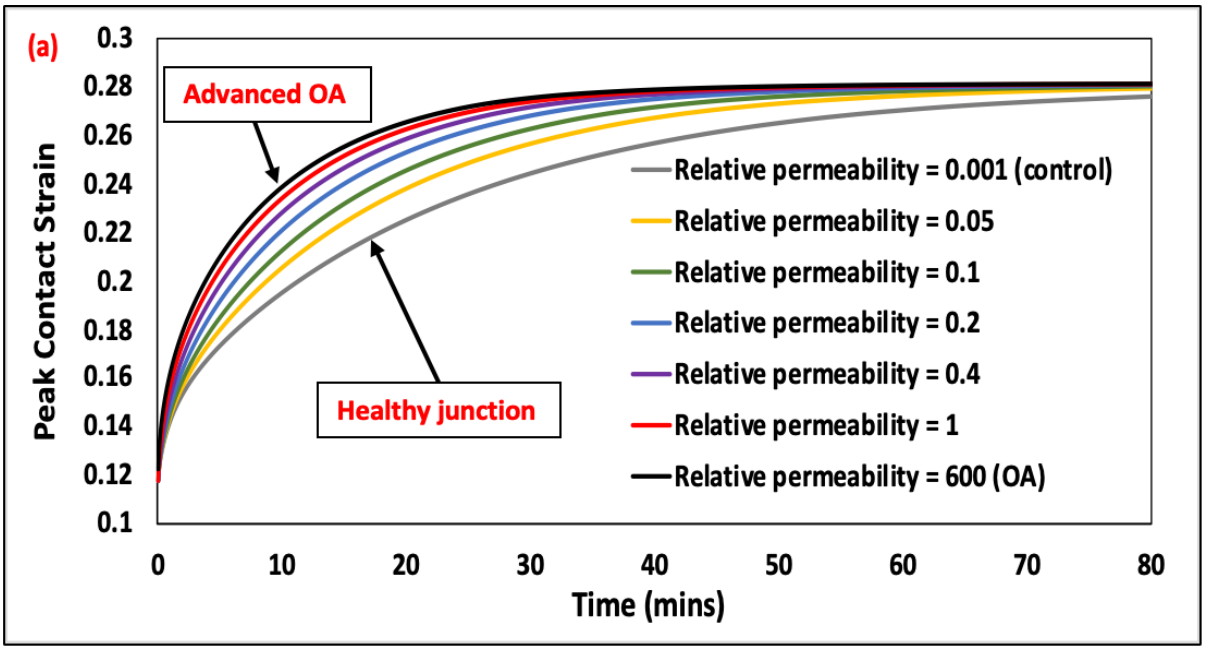
consolidaton time reduces further to 0.8 hours, this is about 60% of the reduction as compared to the control.

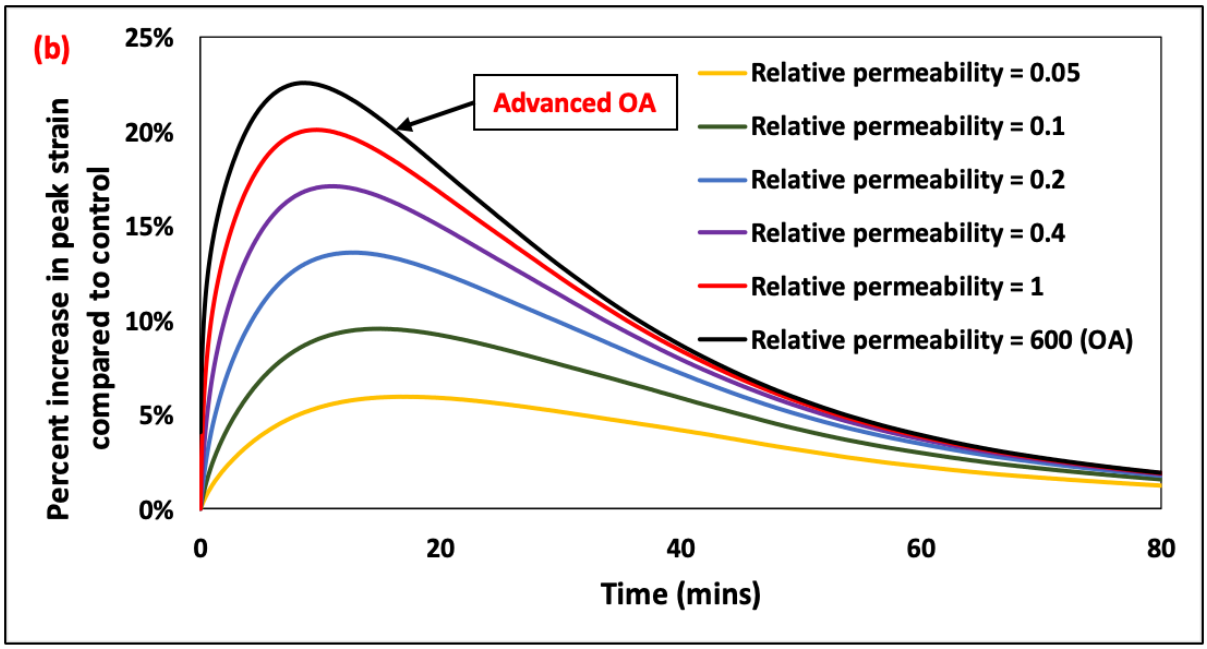
Consolidation for the permeable joint (especially for the diseased joint, i.e. OA) is much faster, as compared to the healthy joint, because of the shorter drainage path (due to the extra escaping pathway via ScBP), it then leads to a quicker excess pore water depletion, this is also presented in figure 4 (d) – (f).

As the tissue experiences a quicker deformation for higher ScBP permeability, larger deformations at the early stage of the loading will also occur. As illustrated in figure 4 (b), at 10 mins after the loading, the peak contact strain is 20% higher as compared to the control for relative permeability ratio of 1, and it is 23% higher under the OA condition when the ratio is larger than 600 which is very significant. Also, the early stage loading deformation (percentage increase relative to the control) increases rapidly from 0 to 20% when the permeability ratio increases from 0.001 to 1. However it only increases from 20% to 23% when the permeability ratio increases from 1 to 600. It shows that the effect of osteochondral junction leakage is greater when the relative permeability ratio increases from 0.001 to 1, and the further increases in ScBP permeability is not promoting any significant effect on the joint lubrication. Figure 4 (c) also confirms this finding, the reduction in fully consolidation time is significant for ratio between 0.001 to 1. However the value starts to converge for further increases of the ScBP permeability.

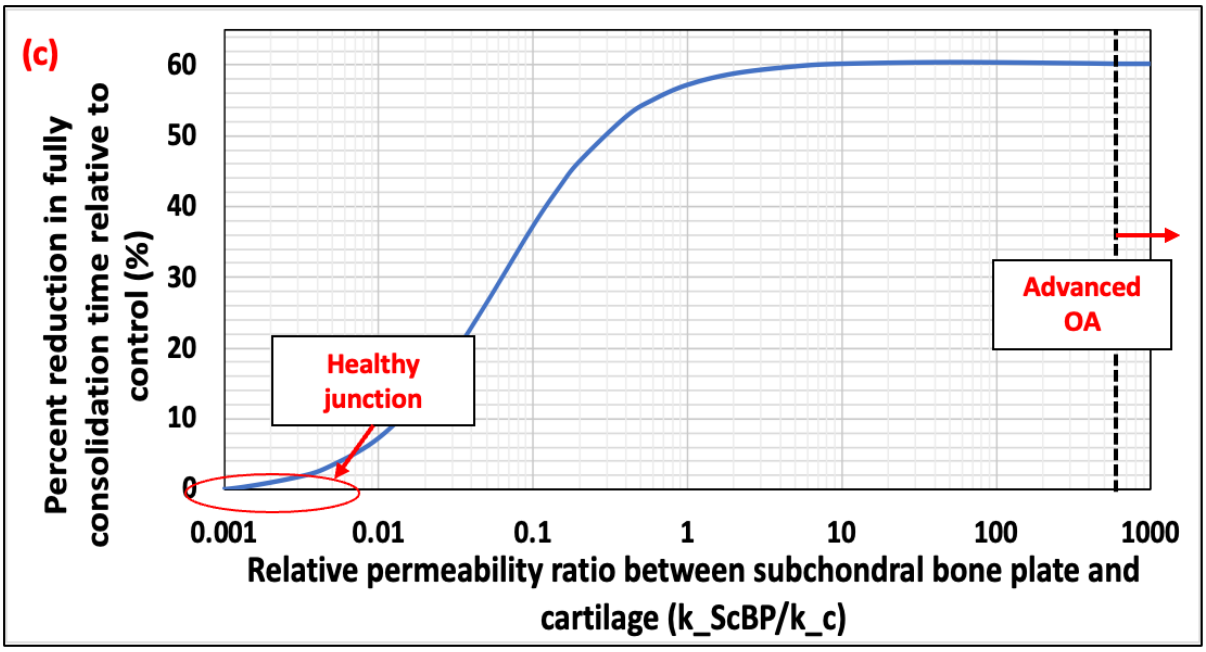
Hydraulic pressure throughout tissue increases effectively instantly with the onset of load to match the load (i.e. the load is initial supported by the fluid in a poroelastic material). Once leakage at the ScBP starts (when the relative permeability ratio increases from 0.001 to 1), the built-up pressure within the tissue and the zero-pressure boundary condition (at the bottome edge of the ScBP) together form a very large pressure gradient, this pressure gradient will drive fluid out of the tissue via the bone plate, the increase in the permeability will give more available cross-sectional area for the fluid to escape. The effect of the increasing ScBP permeability on the tissue deformation and interstitial fluid depresurisation is significant especially when the relative permeability ratio increases from 0.001 (near impermeable) to 1 as presented in figure 4. However, as the ratio continues to increase above 1 (in this study), the effect starts to converge and no much further impact was found in the simulation, which means the impact for the permeable joint on tissue deformation and fluid

depresurisation is similar between the case when the relative permeability ratio is 1 and 600. In the physiological condition (i.e. a real joint), it is not exactly clear at which ratio the effect will converge, because the effect from permeable junction on tissue not only depends on the ScBP permeability, but also the loading conditions, as different physiological activities can generate different pressure gradient at the junction (between tidemark and bottom edge of the ScBP), which can drive the fluid out via ScBP at different rates.

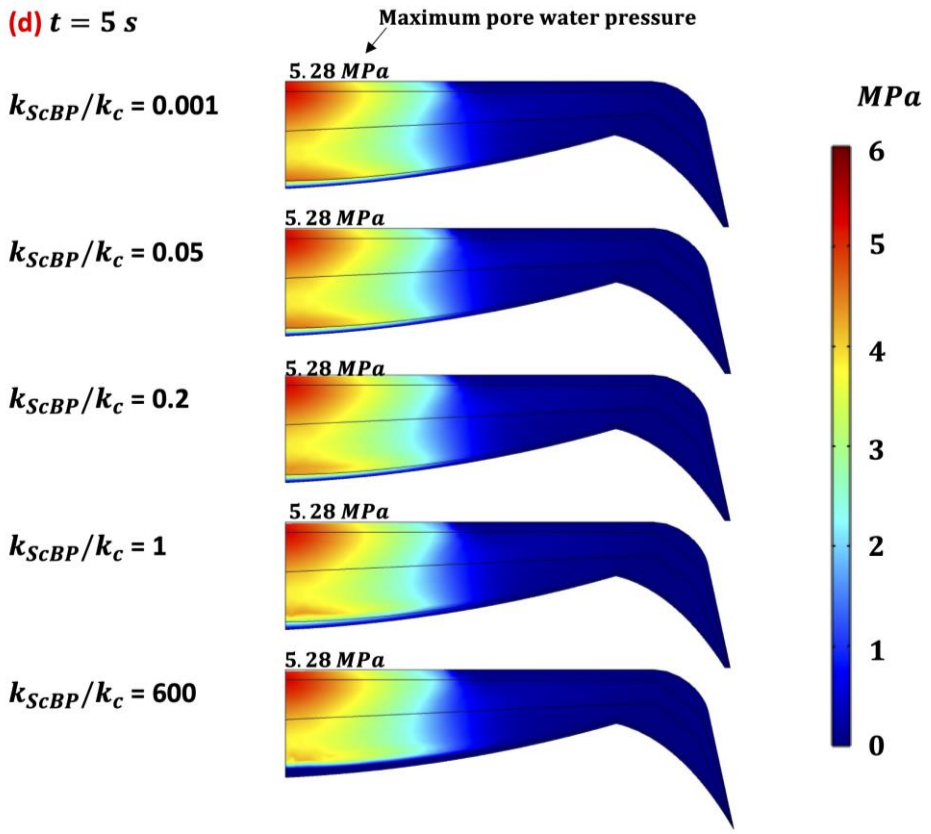


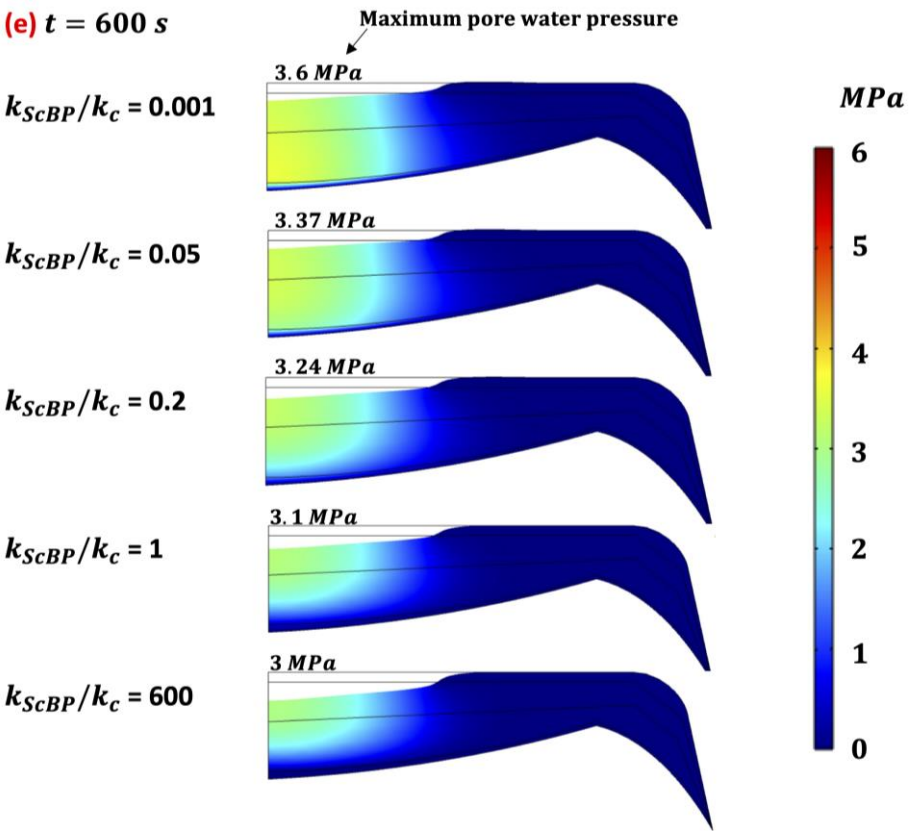


421

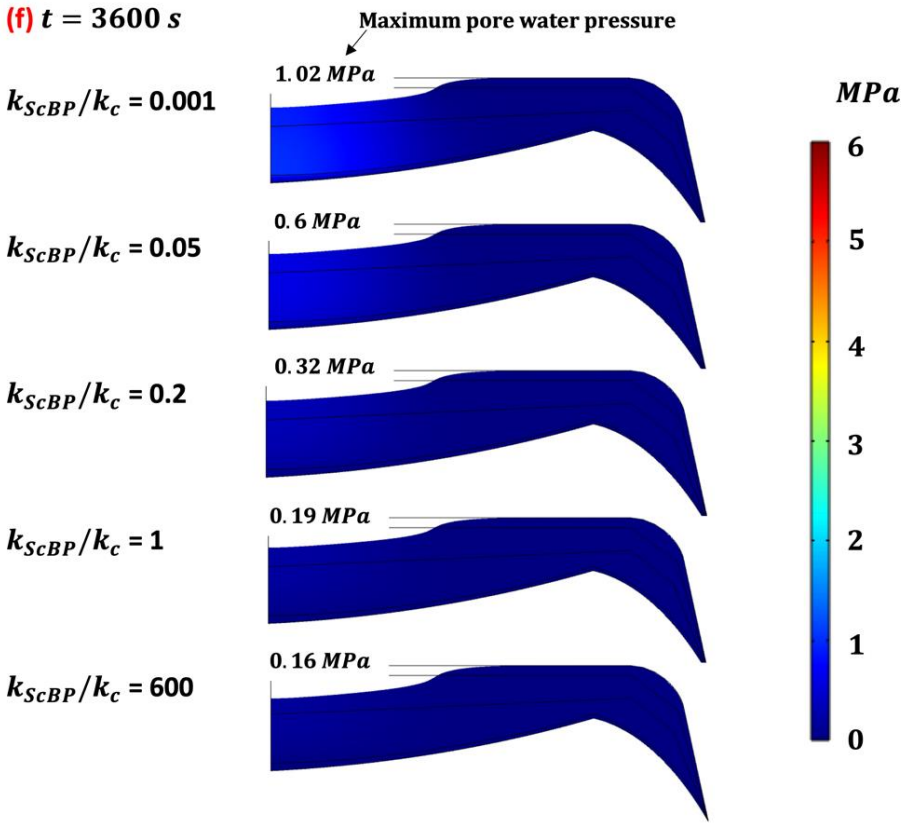

(c)
Percent reduction in fully consolidation time relative to control (%)
60
50
40
30
20
10
0
Healthy junction
Advanced OA
0.001
0.01
0.1
1
10
100
1000
Relative permeability ratio between subchondral bone plate and cartilage (k_ScBP/k_c)

422


(d) $t = 5\ s$
Maximum pore water pressure
5.28 MPa
k_{ScBP}/k_c = 0.001
5.28 MPa
k_{ScBP}/k_c = 0.05
5.28 MPa
k_{ScBP}/k_c = 0.2
5.28 MPa
k_{ScBP}/k_c = 1
5.28 MPa
k_{ScBP}/k_c = 600
MPa
6
5
4
3
2
1
0



423



424

425 **Figure 4: (a) Cartilage tissue peak contact strain for different degrees of relative**

426 **permeability of subchondral bone (K_{ScBP}/K_c); (b) Normalized peak strain for permeable**

osteochondral junction cases compared to control (no leakage allowed); (c) Fully consolidation time versus relative permeability ratio (K_{scbp}/K_c), note, the consolidation time for control case is calculated to be 2 hours; (d) Excess interstitial fluid pressure at t = 5s (e) Excess interstitial fluid pressure at t = 600s, (f) Excess interstitial fluid pressure at t = 3600s.

***Note, for illustration purpose, only a few relative permeability cases are presented in (a) and (b), however, they follow the interpolation trend which can be inferenced from the figures.**

3.2 Lubrication of the cartilage

3.2.1 Friction coefficient

The time-dependent friction coefficient at the point that has maximum contact stress is used in this paper to describe the cartilage tissue lubrication behaviour. It is calculated based on the biphasic lubrication theory [72] and the linear relationship between the degree of consolidation (DoC) and the effective friction coefficient [29] (eq. (28)),

$$\mu_{eff} = \mu_{eq} \times DoC \quad \textbf{(28)}$$

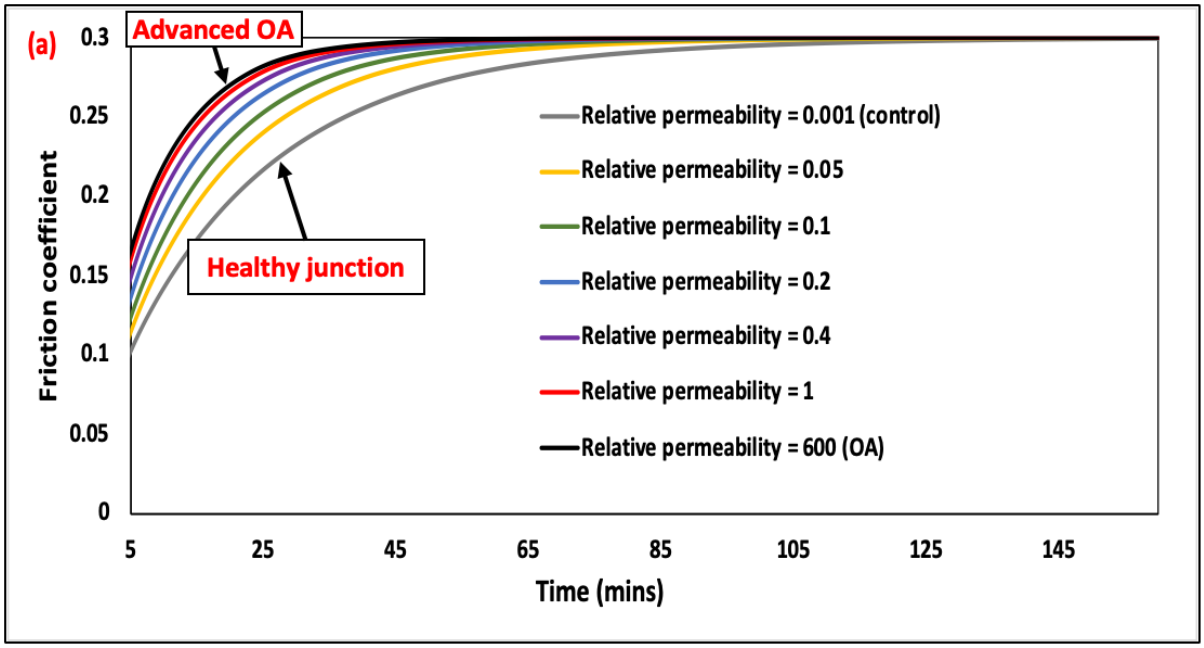
where u_{eff} is the time-dependent effective friction coefficient; μ_{eq} is equilibrium friction coefficient which is assumed to be 0.3 [27].

Experimental studies suggest that it takes several hours (2-3 hrs) for the cartilage response to reach the equilibrium under the compressive loading condition (with one end of the cartilage specimen being impermeable) [27, 73-76]. This timescale is consistent with our modelling prediction for the healthy and normal joints as presented in figure 5(a). On the other hand, for the permeable joints, the amount of time required to reach the elevated friction coefficient is reduced dramatically (by more than half), as compared to the control case.

The earlier increase in friction in compromised joints is due to the large pressure gradient between the tide mark and bottom edge of ScBP, in addition to the short drainage path within the subchondral plate. Once the subchondral bone plate region becomes permeable and deteriorated, the tissue interstitial fluid will escape quickly via this additional path. With more fluid escaping through the osteochondral junction, less fluid will remain pressurized at the superficial layer to resist the applied loading. In addition, the interstitial fluid will be depressurized at a faster rate due to the smaller flow resistance at the subchondral bone plate region. Therefore, cartilage solid to solid contact occurs sooner, resulting in the equilibrium friction coefficient to be reached earlier.

At the early stage of the loading (about 5 mins), the friction coefficient for ScBP permeability at the OA condition is 62% larger than the control, and 57% larger when relative permeability ratio = 1, and 33% larger when relative permeability ratio = 0.2. This finding indicates the significance of the osteochondral junction leakage in the development and progression of osteoarthritis, which is also consistent with the microscopic study performed by Li et al [77],

463 they concluded that the subchondral bone plate that has poorly mineralized and porous bone
464 is a hallmark of osteoarthritis. It is also widely known that the osteochondral junction is a
465 dynamic system in the body [2], the subchondral bone continuously remodels according to
466 the environment (loadings, signals, etc.), the remodelling process cut across the
467 osteochondral interface, and then potentially leakage happens between cartilage and bone.
468 Under normal condition, cartilage tissue produces large quantities of OPG to shut down the
469 bone resorption as the bone remodelling process approaches the cartilage-bone interface and
470 then blocks the bone remodelling [2, 78-82]. However, as people age or for osteoarthritic
471 patients, OPG levels in the cartilage falls, and then the bone remodelling may penetrate closer
472 to the osteochondral interface, and perhaps eventually cross the interface, and lead to the
473 junction leakage. This may represent a positive feedback loop, i.e., as OA progresses, less OPG
474 is secreted, promoting more leakage, leading to higher occurrence of high cartilage contact
475 friction, further promoting the development of the OA.



476

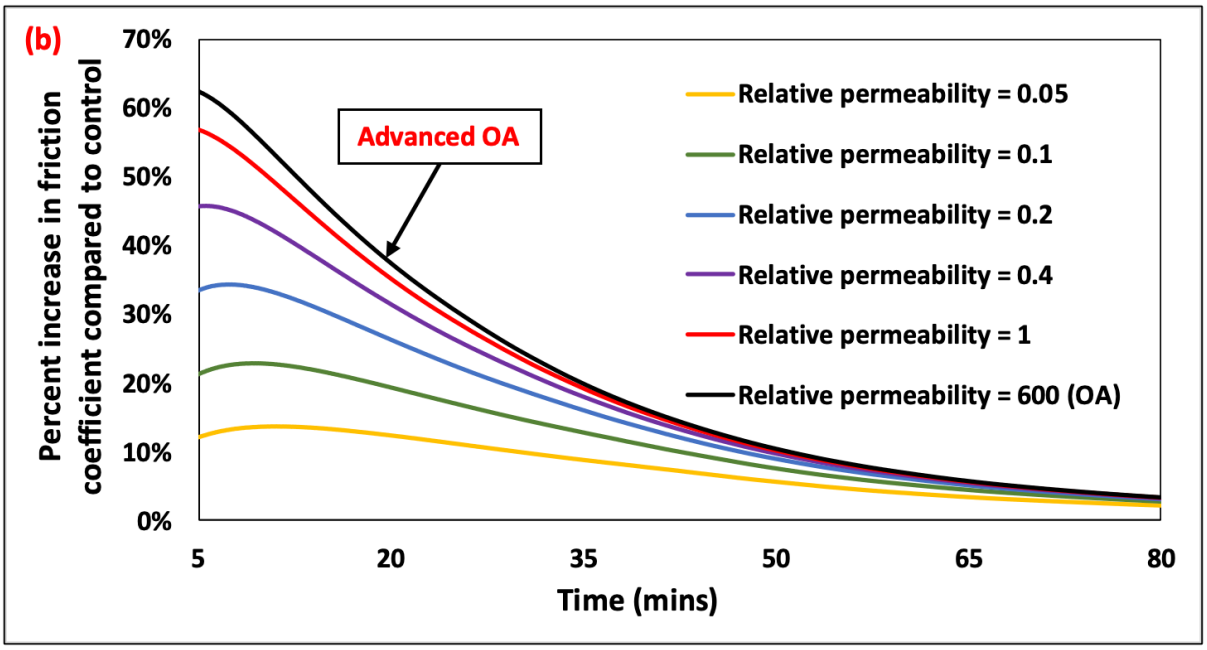


Figure 5: (a) Time-dependent friction coefficient under different relative permeability ratios; (b) Normalized time-dependent friction coefficient for the cases of permeable osteochondral junction compared to control.

3.2.2 Mixed-mode lubrication duration

Figure 6 shows the normalized mixed-mode lubrication duration as compared to the control. As discussed before, mixed-mode lubrication is the joint lubrication regime for most physiological activities [8]. It starts when the surface roughness or asperities make contact and finishes when the fluid pressure at the contact gap is depleted (when contact gap pressure approaches to zero) [1]. It is useful to study the mixed-mode lubrication duration as it is an important indicator of joint health. A shorter mixed-mode lubrication duration indicates the earlier contact for cartilage solid components, and consequently a higher likelihood of cartilage surface wear and osteoarthritis development.

This study predicts the mixed-mode lubrication duration of around 160 mins for a healthy junction, this is in good agreement with the previous study [29], as it takes several hours for the fluid pressurization or friction coefficient to reach an equilibrium value (note, the aggrecan-dependent tissue permeability as shown in eq. (9) was adopted in the study with an average value across the tissue being 2.2e-16 m^4/Ns at the steady state, this is also consistent with the experimental measurements [14, 83]). However, the mixed-mode

lubrication duration reduces significantly once the ScBP starts to leak (as shown in figure 6), the lubrication duration is 33% lower as compared to control when relative permeability = 0.1, 50% lower when relative permeability = 1, and it becomes 52% lower when ScBP permeability is at OA condition. These results suggest a significant reduction in the knee joint lubrication capability under the effect of osteochondral junction leakage, as the load that was initially taken by the fluid is transferred at a faster rate to the solid component of cartialge. When the osteochondral junction becomes permeable and deteriorated, cartilage interstitial fluid escapes via ScBP, less available fluid will go into the contact gap to support the mixed-mode lubrication regime. Together this also reduces the effect of "weeping lubrication" [11, 84]. In the meantime, the fluid drainage path that comes out of the tissue via the contact gap interface also becomes shorter, which also contributes to the reduction of the mixed-mode lubrication duration, and in turn deteriorates the lubrication capability.

As discussed in Section 3.1, the effect of osteochondral junction leakage is most significant when relative permeability is between 0.001 to 1, and further increase in ScBP permeability only has mild effect. This is also seen in the mixed-mode lubrication duration shown in figure 6, where the joint lubricating capability deteriorates most significantly at the early stage of the junction leakage development. Further progression only has mild effect and so the tissue would not deteriorate much further. This finding indicates the importance of early prevention and intervention of the subchondral bone disease, as once the subchondral bone plate becomes permeable, the articular joint could suffers significant loss of its lubrication capability and functionality.

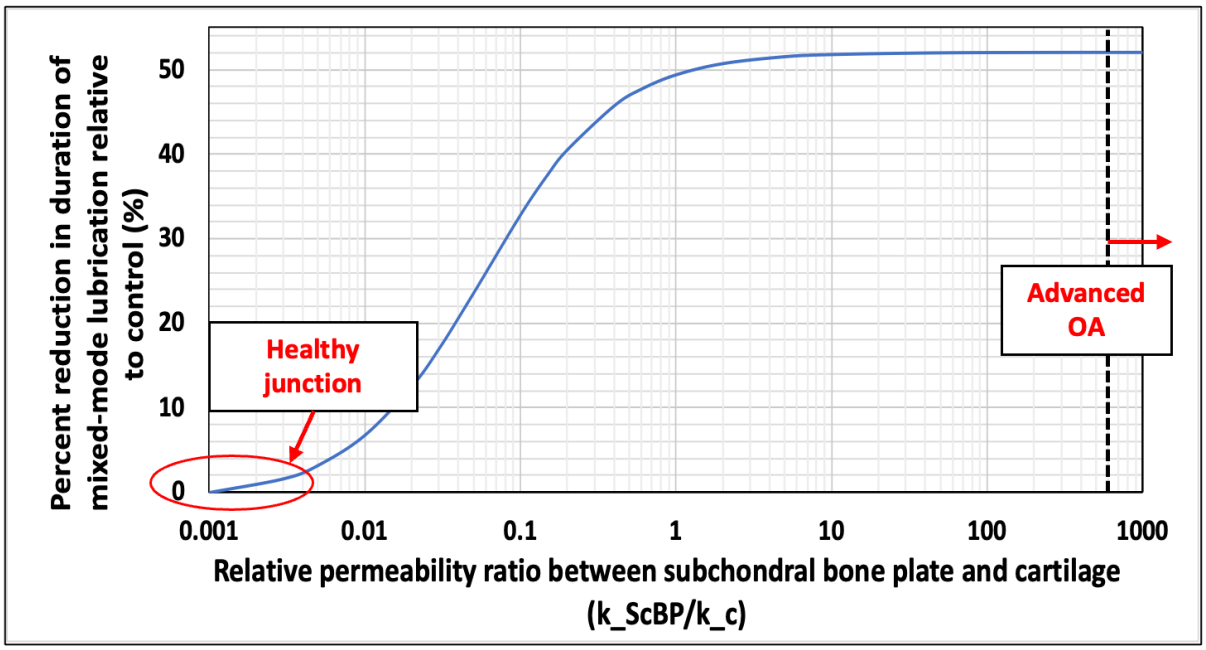


Figure 6: Normalized mixed-mode lubrication duration compared to control for different relative permeability ratios between the subchondral bone plate to cartilage (k_{scbp}/k_c)

4 Limitations

A few limitations in the study should be noted. First, the current study uses static compressive loading to investigate the effect of osteochondral junction leakage on joint lubrication behaviour, it serves as the first step in the investigation. In the future study, a dynamic loading with different frequencies and speeds (to simulate walking and running) can be used to better understand how a diseased osteochondral junction affects the joint. Second, an axis-symmetrical geometry and coordinates are employed to simplify the problem. We do expect additional variations due to the presence of the meniscus, ligaments, and joint contact geometry to also affect the fluid flow behaviour in the gap junction. In future studies, improvement can be made by constructing a 3D model of the knee joints based on CT scan images to account for these geometrical variables. Third, this study assumes the constant synovial fluid viscosity. It is acceptable to adopt for constant value for the static compression loading as a first approximation to steady state conditions, however, more complex rheology of synovial fluid can be built into the model for a more realistic scenario modelling. Lastly, this study estimates the permeability ratio between the subchondral bone plate and cartilage based on the subchondral bone plate's porosity. In future studies, improvement can be made

by replacing these estimates with experimental data to make these theoretical predictions closer to reality.

5 Conclusion

This study investigated the cartilage lubrication but focused on the potential impact of osteochondral junction leakage. In addition, the effect of the meniscus on fluid flow in the contact gap was also considered in the modelling. The main conclusions are summarized as follows:

- The effect of osteochondral junction leakage is significant on cartilage joint lubrication, and it is most apparent during the early stage of the junction leakage development (when relative permeability is between 0.001 to 1.0 in this study).
- The model predicts that normal adult knee cartilage could take about 2 hours for a healthy cartilage tissue to reach steady-state consolidation. However, the full consolidation time reduces to 1.2 hours when relative permeability ratio = 0.1 (early stage of osteochondral junction leakage). It reduces to 0.8 hours when ScBP permeability is at the OA condition, this is equivalent to a 60% reduction.
- The time-dependent friction coefficient rises sooner with the increasing subchondral bone plate permeability (as the osteochondral junction leakage deteriorates). As compared to control, the initial friction coefficient increases by 62% for ScBP permeability at the OA condition, and 57% when relative permeability ratio = 1, and 33% when relative permeability ratio = 0.2. This result indicates the potential for a significant contribution of a leaky osteochondral junction on the development of knee diseases, such as osteoarthritis.
- The mixed-mode lubrication duration and the joint lubrication capability is reduced significantly when the ScBP becomes permeable (at early stage of osteochondral junction leakage). As compared to control, the mixed-mode lubrication is 33% lower when relative permeability = 0.1, and 50% lower when relative permeability = 1, and it becomes 52% lower when ScBP permeability is at OA condition. These results suggest a significant reduction in the knee joint lubrication under the effect of osteochondral junction leakage.

- Early intervention (*e.g.,* following sports injury) to prevent osteoarthritic subchondral bone disease may be justified because once the subchondral bone plate becomes permeable, the articular joint is likely to suffer significant loss in terms of its lubrication capability, increased wear, and consequent loss of functionality.

6 Acknowledgements

The authors acknowledge the funding support from The Australian Research Council (DP180100915) and The University of Melbourne

7 Conflict of interest

The authors declare that they have no known competing financial interests or personal relationships that could have appeared to influence the work reported in this paper.

8 Reference

[1] J. Liao, D.W. Smith, S. Miramini, B.S. Gardiner, L. Zhang, A coupled contact model of cartilage lubrication in the mixed-mode regime under static compression, Tribology International, 145 (2020) 106185.
[2] D. Smith, B. Gardiner, L. Zhang, A. Grodzinsky, Articular Cartilage Dynamics, 2019.
[3] N. Canter, BAM: Antiwear and friction-reducing coating, Tribology & Lubrication Technology, 65 (2009) 14.
[4] D. Flom, N. Porile, Friction of teflon sliding on teflon, Journal of Applied Physics, 26 (1955) 1088-1092.
[5] W. Lin, J. Klein, Recent progress in cartilage lubrication, Advanced Materials, 33 (2021) 2005513.
[6] Z. Jin, J. Fisher, 2 - Tribology in joint replacement*Note: This chapter is an updated version of Chapter 2, from the first edition of Joint replacement technology, edited by P. A. Revell and published by Woodhead Publishing, 2008*, in: P.A. Revell (Ed.) Joint Replacement Technology (Second Edition), Woodhead Publishing2014, pp. 31-61.
[7] D. Dowson, V. Wright, M.D. Longfield, Human joint lubrication, Biomed Eng, 4 (1969) 160-165.
[8] C.P. Neu, K. Komvopoulos, A.H. Reddi, The interface of functional biotribology and regenerative medicine in synovial joints, Tissue Eng Part B Rev, 14 (2008) 235-247.
[9] M. Daniel, Boundary cartilage lubrication: review of current concepts, Wien Med Wochenschr, 164 (2014) 88-94.
[10] G.A. Ateshian, Biphasic Lubrication, in: Q.J. Wang, Y.-W. Chung (Eds.) Encyclopedia of Tribology, Springer US, Boston, MA, 2013, pp. 226-233.

[11] P.R. Lewis, C.W. McCutchen, Mechanism of Animal Joints: Experimental Evidence for Weeping Lubrication in Mammalian Joints, Nature, 184 (1959) 1285-1285.
[12] C.W. McCutchen, Mechanism of Animal Joints: Sponge-hydrostatic and Weeping Bearings, Nature, 184 (1959) 1284-1285.
[13] T.D. Brower, Y. Akahoshi, P. Orlic, The Diffusion of Dyes Through Articular Cartilage in Vivo, JBJS, 44 (1962) 456-463.
[14] A. Maroudas, P. Bullough, Permeability of Articular Cartilage, Nature, 219 (1968) 1260-1261.
[15] R. Honner, R.C. Thompson, The nutritional pathways of articular cartilage. An autoradiographic study in rabbits using 35S injected intravenously, J Bone Joint Surg Am, 53 (1971) 742-748.
[16] K. Ogata, L.A. Whiteside, Barrier to material transfer at the bone-cartilage interface: measurement with hydrogen gas in vivo, Clin Orthop Relat Res, (1979) 273-276.
[17] G. Li, J. Yin, J. Gao, T.S. Cheng, N.J. Pavlos, C. Zhang, M.H. Zheng, Subchondral bone in osteoarthritis: insight into risk factors and microstructural changes, Arthritis Research & Therapy, 15 (2013) 223.
[18] X.L. Yuan, H.Y. Meng, Y.C. Wang, J. Peng, Q.Y. Guo, A.Y. Wang, S.B. Lu, Bone-cartilage interface crosstalk in osteoarthritis: potential pathways and future therapeutic strategies, Osteoarthritis Cartilage, 22 (2014) 1077-1089.
[19] E. Martín-Badosa, D. Amblard, S. Nuzzo, A. Elmoutaouakkil, L. Vico, F. Peyrin, Excised bone structures in mice: imaging at three-dimensional synchrotron radiation micro CT, Radiology, 229 (2003) 921-928.
[20] P. Schneider, T. Krucker, E. Meyer, A. Ulmann-Schuler, B. Weber, M. Stampanoni, R. Müller, Simultaneous 3D visualization and quantification of murine bone and bone vasculature using micro-computed tomography and vascular replica, Microsc Res Tech, 72 (2009) 690-701.
[21] P. Schneider, M. Stauber, R. Voide, M. Stampanoni, L.R. Donahue, R. Müller, Ultrastructural properties in cortical bone vary greatly in two inbred strains of mice as assessed by synchrotron light based micro- and nano-CT, J Bone Miner Res, 22 (2007) 1557-1570.
[22] B. Pouran, V. Arbabi, R.L. Bleys, P. René van Weeren, A.A. Zadpoor, H. Weinans, Solute transport at the interface of cartilage and subchondral bone plate: Effect of micro-architecture, J Biomech, 52 (2017) 148-154.
[23] A. Malandrino, D. Lacroix, C. Hellmich, K. Ito, S.J. Ferguson, J. Noailly, The role of endplate poromechanical properties on the nutrient availability in the intervertebral disc, Osteoarthritis Cartilage, 22 (2014) 1053-1060.
[24] G. Gailani, M. Benalla, R. Mahamud, S.C. Cowin, L. Cardoso, Experimental determination of the permeability in the lacunar-canalicular porosity of bone, J Biomech Eng, 131 (2009) 101007.
[25] J. Hwang, W.C. Bae, W. Shieu, C.W. Lewis, W.D. Bugbee, R.L. Sah, Increased hydraulic conductance of human articular cartilage and subchondral bone plate with progression of osteoarthritis, Arthritis Rheum, 58 (2008) 3831-3842.
[26] A. Malandrino, D. Lacroix, C. Hellmich, K. Ito, S.J. Ferguson, J. Noailly, The role of endplate poromechanical properties on the nutrient availability in the intervertebral disc, Osteoarthritis and Cartilage, 22 (2014) 1053-1060.
[27] G.A. Ateshian, The role of interstitial fluid pressurization in articular cartilage lubrication, J Biomech, 42 (2009) 1163-1176.

[28] L. Zhang, B.S. Gardiner, D.W. Smith, P. Pivonka, A.J. Grodzinsky, The effect of cyclic deformation and solute binding on solute transport in cartilage, Archives of biochemistry and biophysics, 457 1 (2007) 47-56.
[29] S. Miramini, D.W. Smith, L. Zhang, B.S. Gardiner, The spatio-temporal mechanical environment of healthy and injured human cartilage during sustained activity and its role in cartilage damage, J Mech Behav Biomed Mater, 74 (2017) 1-10.
[30] L. Zhang, S. Miramini, D.W. Smith, B.S. Gardiner, A.J. Grodzinsky, Time evolution of deformation in a human cartilage under cyclic loading, Ann Biomed Eng, 43 (2015) 1166-1177.
[31] S. Beeler, L. Vlachopoulos, L. Jud, R. Sutter, T. Götschi, P. Fürnstahl, S.F. Fucentese, Meniscus sizing using three-dimensional models of the ipsilateral tibia plateau based on CT scans - an experimental study of a new sizing approach, J Exp Orthop, 7 (2020) 36.
[32] J.M. Marzo, J. Gurske-DePerio, Effects of medial meniscus posterior horn avulsion and repair on tibiofemoral contact area and peak contact pressure with clinical implications, Am J Sports Med, 37 (2009) 124-129.
[33] L. Zhang, M. Richardson, P. Mendis, Role of chemical and mechanical stimuli in mediating bone fracture healing, Clinical and Experimental Pharmacology and Physiology, 39 (2012) 706-710.
[34] M.K. Barker, B.B. Seedhom, The relationship of the compressive modulus of articular cartilage with its deformation response to cyclic loading: does cartilage optimize its modulus so as to minimize the strains arising in it due to the prevalent loading regime?, Rheumatology, 40 (2001) 274-284.
[35] L. Zhang, B.S. Gardiner, D.W. Smith, P. Pivonka, A. Grodzinsky, The effect of cyclic deformation and solute binding on solute transport in cartilage, Arch Biochem Biophys, 457 (2007) 47-56.
[36] G.A. Ateshian, M.A. Soltz, R.L. Mauck, I.M. Basalo, C.T. Hung, W. Michael Lai, The Role of Osmotic Pressure and Tension-Compression Nonlinearity in the Frictional Response of Articular Cartilage, Transport in Porous Media, 50 (2003) 5-33.
[37] M.A. Soltz, G.A. Ateshian, A Conewise Linear Elasticity mixture model for the analysis of tension-compression nonlinearity in articular cartilage, J Biomech Eng, 122 (2000) 576-586.
[38] V.C. Mow, S.C. Kuei, W.M. Lai, C.G. Armstrong, Biphasic creep and stress relaxation of articular cartilage in compression? Theory and experiments, J Biomech Eng, 102 (1980) 73-84.
[39] L. Zhang, D.W. Smith, B.S. Gardiner, A.J. Grodzinsky, Modeling the Insulin-Like Growth Factor System in Articular Cartilage, PLoS One, 8 (2013).
[40] L. Zhang, Gardiner, Smith, Pivonka, Grodzinsky, On the role of diffusible binding partners in modulating the transport and concentration of proteins in tissues, Journal of Theoretical Biology, 263 (2010) 20--29.
[41] L. Zhang, S. Miramini, D.W. Smith, B.S. Gardiner, A.J. Grodzinsky, Time Evolution of Deformation in a Human Cartilage Under Cyclic Loading, Annals of Biomedical Engineering, 43 (2015) 1166-1177.
[42] A. Curnier, Q.-C. He, P. Zysset, Conewise linear elastic materials, Journal of Elasticity, 37 (1994) 1-38.
[43] A. Maroudas, E. Wachtel, G. Grushko, E.P. Katz, P. Weinberg, The effect of osmotic and mechanical pressures on water partitioning in articular cartilage, Biochim Biophys Acta, 1073 (1991) 285-294.
[44] S. Treppo, H. Koepp, E.C. Quan, A.A. Cole, K.E. Kuettner, A.J. Grodzinsky, Comparison of biomechanical and biochemical properties of cartilage from human knee and ankle pairs, J Orthop Res, 18 (2000) 739-748.

[45] Y. Xia, S. Zheng, A. Bidthanapally, Depth-dependent profiles of glycosaminoglycans in articular cartilage by microMRI and histochemistry, J Magn Reson Imaging, 28 (2008) 151-157.
[46] G.E. Kempson, H. Muir, C. Pollard, M. Tuke, The tensile properties of the cartilage of human femoral condyles related to the content of collagen and glycosaminoglycans, Biochim Biophys Acta, 297 (1973) 456-472.
[47] L. Zhang, Solute transport in cyclic deformed heterogeneous articular cartilage, International Journal of Applied Mechanics, 3 (2011) 507--524.
[48] L. Zhang, B. Gardiner, D. Smith, P. Pivonka, A. Grodzinsky, Integrated model of IGF-I mediated biosynthesis in a deformed articular cartilage, Journal of Engineering Mechanics, 135 (2009) 439--449.
[49] L. Zhang, B. Gardiner, D. Smith, P. Pivonka, A. Grodzinsky, A fully coupled poroelastic reactive-transport model of cartilage, Molecular & Cellular Biomechanics, 5 (2008) 133--153.
[50] L. Zhang, B. Gardiner, D. Smith, P. Pivonka, A. Grodzinsky, IGF uptake with competitive binding in articular cartilage, Journal of Biological Systems, 16 (2008) 175--195.
[51] L. Zhang, B. Gardiner, D. Smith, P. Pivonka, J. Grodzinsky, The effect of cyclic deformation and solute binding on solute transport in cartilage, Archives of Biochemistry and Biophysics, 457 (2007) 47--56.
[52] L. Bonassar, A. Grodzinsky, A. Srinivasan, S. Davila, S. Trippel, Mechanical and Physicochemical Regulation of the Action of Insulin-Like Growth Factor-I on Articular Cartilage, Archives of biochemistry and biophysics, 379 (2000) 57-63.
[53] O. Zamparo, W.D. Comper, Hydraulic conductivity of chondroitin sulfate proteoglycan solutions, Archives of Biochemistry and Biophysics, 274 (1989) 259-269.
[54] J. Liao, D.W. Smith, S. Miramini, B.S. Gardiner, L. Zhang, A Probabilistic Failure Risk Approach to The Problem of Articular Cartilage Lubrication, Computer Methods and Programs in Biomedicine, 203 (2021) 106053.
[55] J. Liao, D.W. Smith, S. Miramini, N. Thibbotuwawa, B.S. Gardiner, L. Zhang, The investigation of fluid flow in cartilage contact gap, Journal of the Mechanical Behavior of Biomedical Materials, 95 (2019) 153-164.
[56] J.M. Deneweth, K.E. Newman, S.M. Sylvia, S.G. McLean, E.M. Arruda, Heterogeneity of tibial plateau cartilage in response to a physiological compressive strain rate, J Orthop Res, 31 (2013) 370-375.
[57] D.L. Robinson, M.E. Kersh, N.C. Walsh, D.C. Ackland, R.N. de Steiger, M.G. Pandy, Mechanical properties of normal and osteoarthritic human articular cartilage, J Mech Behav Biomed Mater, 61 (2016) 96-109.
[58] S. Graindorge, W. Ferrandez, Z. Jin, E. Ingham, C. Grant, P. Twigg, J. Fisher, Biphasic surface amorphous layer lubrication of articular cartilage, Medical Engineering & Physics, 27 (2005) 836-844.
[59] J. Martel-Pelletier, D. Lajeunesse, P. Reboul, J.-P. Pelletier, Chapter 2 - The Role of Subchondral Bone in Osteoarthritis, in: L. Sharma, F. Berenbaum (Eds.) Osteoarthritis, Mosby, Philadelphia, 2007, pp. 15-32.
[60] S. Milz, R. Putz, Quantitative morphology of the subchondral plate of the tibial plateau, Journal of anatomy, 185 (Pt 1) (1994) 103-110.
[61] D. Lacroix, P.J. Prendergast, A mechano-regulation model for tissue differentiation during fracture healing: analysis of gap size and loading, J Biomech, 35 (2002) 1163-1171.
[62] X. Liu, S. Miramini, M. Patel, J. Liao, D. Shidid, L. Zhang, Influence of therapeutic grip exercises induced loading rates in distal radius fracture healing with volar locking plate fixation, Computer Methods and Programs in Biomedicine, 215 (2022) 106626.

[63] D.W. Goodwin, Y.Z. Wadghiri, H. Zhu, C.J. Vinton, E.D. Smith, J.F. Dunn, Macroscopic structure of articular cartilage of the tibial plateau: influence of a characteristic matrix architecture on MRI appearance, AJR Am J Roentgenol, 182 (2004) 311-318.
[64] M.A.J. Finnilä, J. Thevenot, O.M. Aho, V. Tiitu, J. Rautiainen, S. Kauppinen, M.T. Nieminen, K. Pritzker, M. Valkealahti, P. Lehenkari, S. Saarakkala, Association between subchondral bone structure and osteoarthritis histopathological grade, J Orthop Res, 35 (2017) 785-792.
[65] H.L. Stewart, C.E. Kawcak, The Importance of Subchondral Bone in the Pathophysiology of Osteoarthritis, Front Vet Sci, 5 (2018) 178.
[66] I. Kutzner, B. Heinlein, F. Graichen, A. Bender, A. Rohlmann, A. Halder, A. Beier, G. Bergmann, Loading of the knee joint during activities of daily living measured in vivo in five subjects, J Biomech, 43 (2010) 2164-2173.
[67] C.E. Metzger, D.B. Burr, M.R. Allen, Anatomy and Structural Considerations, in: M. Zaidi (Ed.) Encyclopedia of Bone Biology, Academic Press, Oxford, 2020, pp. 218-232.
[68] K. Rogers, Encyclopedia Britannica, The Editors of Encyclopaedia Britannica, 2015.
[69] X. Zhu, Y.T. Chan, P.S.H. Yung, R.S. Tuan, Y. Jiang, Subchondral Bone Remodeling: A Therapeutic Target for Osteoarthritis, Front Cell Dev Biol, 8 (2020) 607764.
[70] H. Madry, C.N. van Dijk, M. Mueller-Gerbl, The basic science of the subchondral bone, Knee Surg Sports Traumatol Arthrosc, 18 (2010) 419-433.
[71] A. Hosseini, S.K. Van de Velde, M. Kozanek, T.J. Gill, A.J. Grodzinsky, H.E. Rubash, G. Li, In-vivo time-dependent articular cartilage contact behavior of the tibiofemoral joint, Osteoarthritis Cartilage, 18 (2010) 909-916.
[72] G.A. Ateshian, A theoretical formulation for boundary friction in articular cartilage, J Biomech Eng, 119 (1997) 81-86.
[73] R. Krishnan, M. Kopacz, G.A. Ateshian, Experimental verification of the role of interstitial fluid pressurization in cartilage lubrication, J Orthop Res, 22 (2004) 565-570.
[74] H. Forster, J. Fisher, The Influence of Loading Time and Lubricant on the Friction of Articular Cartilage, Proceedings of the Institution of Mechanical Engineers, Part H: Journal of Engineering in Medicine, 210 (1996) 109-119.
[75] M.J. Carter, I.M. Basalo, G.A. Ateshian, The temporal response of the friction coefficient of articular cartilage depends on the contact area, J Biomech, 40 (2007) 3257-3260.
[76] A. Oloyede, N.D. Broom, Is classical consolidation theory applicable to articular cartilage deformation?, Clin Biomech (Bristol, Avon), 6 (1991) 206-212.
[77] B. Li, D. Marshall, M. Roe, R.M. Aspden, The electron microscope appearance of the subchondral bone plate in the human femoral head in osteoarthritis and osteoporosis, J Anat, 195 (Pt 1) (1999) 101-110.
[78] S. Shimizu, Y. Asou, S. Itoh, U.I. Chung, H. Kawaguchi, K. Shinomiya, T. Muneta, Prevention of cartilage destruction with intraarticular osteoclastogenesis inhibitory factor/osteoprotegerin in a murine model of osteoarthritis, Arthritis Rheum, 56 (2007) 3358-3365.
[79] S.K. Tat, J.P. Pelletier, C.R. Velasco, M. Padrines, J. Martel-Pelletier, New perspective in osteoarthritis: the OPG and RANKL system as a potential therapeutic target?, Keio J Med, 58 (2009) 29-40.
[80] A.R. Upton, C.A. Holding, A.A. Dharmapatni, D.R. Haynes, The expression of RANKL and OPG in the various grades of osteoarthritic cartilage, Rheumatol Int, 32 (2012) 535-540.
[81] B. Bolon, M. Grisanti, K. Villasenor, S. Morony, U. Feige, W.S. Simonet, Generalized Degenerative Joint Disease in Osteoprotegerin (Opg) Null Mutant Mice, Vet Pathol, 52 (2015) 873-882.

792 [82] B. Kovács, E. Vajda, E.E. Nagy, Regulatory Effects and Interactions of the Wnt and OPG-
793 RANKL-RANK Signaling at the Bone-Cartilage Interface in Osteoarthritis, International Journal
794 of Molecular Sciences, 20 (2019) 4653.
795 [83] F. Boschetti, G.M. Peretti, M. Colombo, S. Cattaneo, R. Pietrabissa, F. Gervaso, G.
796 Fraschini, Direct and indirect measurement of human articular cartilage permeability, 2004.
797 [84] S.M. McNary, K.A. Athanasiou, A.H. Reddi, Engineering lubrication in articular cartilage,
798 Tissue Eng Part B Rev, 18 (2012) 88-100.

799

Title: Osteochondral junction leakage and cartilage joint lubrication

Qin Li
Department of Infrastructure Engineering,
The University of Melbourne, Victoria 3010, Australia
Email: qinl3@student.unimelb.edu.au

Dr Saeed Miramini
Department of Infrastructure Engineering,
The University of Melbourne, Victoria 3010, Australia
Email: s.miramini@unimelb.edu.au

Professor David Smith
School of Physics, Mathematics and Computing,
The University of Western Australia, WA 6009, Australia
Email: David.smith@uwa.edu.au

Professor Bruce Gardiner
Centre for Molecular Medicine and Innovative Therapeutics
Murdoch University, WA 6150, Australia
Email: B.Gardiner@murdoch.edu.au

Professor Lihai Zhang
Department of Infrastructure Engineering,
The University of Melbourne, Victoria 3010, Australia
Email: lihzhang@unimelb.edu.au